Geophysical Research Letters

RESEARCH LETTER
10.1029/2022GL101217

A Shifting Tripolar Pattern of Antarctic Sea Ice Concentration Anomalies During Multi-Year La Niña Events

Tingting Zhu[1] **and Jin-Yi Yu**[1]

[1]Department of Earth System Science, University of California Irvine, Irvine, CA, USA

Key Points:

- The typical sea ice anomaly pattern appears during the second winter of multi-year La Niñas but was zonally shifted during the first winter
- The shifted pattern results from an unique pre-onset Indian ocean condition of multi-year La Niña and atmospheric teleconnections it excites
- The different sea ice impacts revealed in the CESM1 simulation appear in four of the six observed multi-year La Niña events during 1979–2020

Supporting Information:

Supporting Information may be found in the online version of this article.

Correspondence to:

J.-Y. Yu,
jyyu@uci.edu

Citation:

Zhu, T., & Yu, J.-Y. (2022). A shifting tripolar pattern of Antarctic sea ice concentration anomalies during multi-year La Niña events. *Geophysical Research Letters*, *49*, e2022GL101217. https://doi.org/10.1029/2022GL101217

Received 12 SEP 2022
Accepted 25 OCT 2022

Author Contributions:

Funding acquisition: Jin-Yi Yu
Investigation: Tingting Zhu
Project Administration: Jin-Yi Yu
Supervision: Jin-Yi Yu
Visualization: Tingting Zhu
Writing – original draft: Tingting Zhu
Writing – review & editing: Jin-Yi Yu

Abstract A 2,200-year CESM1 pre-industrial simulation is used to contrast Antarctic sea ice concentration (SIC) variations between the first and second austral winters of multi-year La Niñas. The typical SIC anomaly pattern induced by single-year La Niñas appears only during the second austral winter of multi-year La Niñas. A similar pattern, but zonally shifted compared to the typical one, is found during the first winter and exhibits a tripolar pattern with anomaly centers over the Ross, Amundsen-Bellingshausen, and Weddell Seas. The shift is a result of the pre-onset conditions associated with multi-year La Niñas that excites unique atmospheric circulation modes during the first winter. The distinct zonally-shifted SIC anomaly pattern is observed in four of the six multi-year La Niña events during the period 1979–2020. These results suggest that it is helpful to separate La Niñas into single and multi-year events to better understand the La Niña impacts on Antarctic climate.

Plain Language Summary La Niña events are characterized by abnormal cooling of sea surface waters in the tropical Pacific Ocean. Recently, more La Niña events have been observed to persist for multiple year. In this study, we analyze a long-term climate model simulation to show that multi-year La Niñas produce a different impact on Antarctic sea ice concentrations (SIC) than single-year La Niñas. The typical SIC impact produced by single-year La Niñas appears only during the second austral winter of multi-year La Niñas. In contrast, during the first winter of multi-year La Niñas the pattern is shifted westward and is characterized by a distinct tripolar pattern with anomaly centers over the Ross, Amundsen-Bellingshausen, Weddell Seas. The different impact pattern during the first winter is caused by the different atmospheric wave trains excited by the different Indian Ocean conditions during the first and second winters of multi-year events. The distinct impacts and impact mechanisms found in the climate model are also found in the observations. Four out of the six multi-year La Niña events observed during 1979–2020 exhibit this zonally-shifted SIC anomaly pattern during their first winters. The increasing occurrence of multi-year La Niña events may affect Antarctic sea ice patterns in new ways.

1. Introduction

El Niño-Southern Oscillation (ENSO) events typically develop during the June-July-August (JJA) season, peak during the following December-January-February (DJF) and decay during the immediately following March-April-May (MAM) season. As such, ENSO events usually last for about 1 year. However, some ENSO events persist and even re-intensify in the following year to become multi-year events. Multi-year events happen more frequently for the cold phase (La Niña) of ENSO than for the warm phase (El Niño) (Hu et al., 2014; Okumura & Deser, 2010). An increasing amount of interest and effort is being made to understand the underlying dynamics of multi-year La Niña events (and more generally, multi-year ENSOs) and their possible unique climate impacts. Studies have shown that multi-year La Niñas can induce more severe climate impacts than single-year La Niñas. Okumura et al. (2017) found that multi-year La Niñas caused severe U.S. drought during their second boreal winter by strengthening atmospheric circulation anomalies. Iwakiri and Watanabe (2020) found that the warm summer induced by the multi-year La Niña over Japan during the second year of the event is spatially different in its anomaly pattern from that during the first summer of the event.

These recent research efforts focused on the impacts of multi-year La Niñas on northern hemisphere climate. Possible different impacts on southern hemisphere climate are yet to be identified. ENSO events are known to be capable of affecting interannual variations of Antarctic sea ice concentration (SIC) by altering the atmospheric general circulation and large-scale wave propagation (e.g., Liu et al., 2002; Nuncio & Yuan, 2015; Yuan, 2004; Yuan et al., 2018). La Niña events typically induce a SIC anomaly dipole around western Antarctic during the

austral winter season (i.e., JJA) by weakening the Amundsen Sea Low (Yuan, 2004). Previous studies mostly used composite and linear regression/correlation analyses to identify the La Niña impacts, which mixed the impacts produced by single and multi-year events. There is a need to examine and contrast the La Niña impacts on Antarctic SICs between single and multi-year events. Previous studies have suggested that multi-year La Niña events differ from single-year events in that they tend to be preceded by a strong El Niño event (Iwakiri & Watanabe, 2021) and accompanied by a different Indian Ocean Dipole (IOD) compared to single-year events (Kim & Yu, 2022). These different properties may cause the multi-year La Niñas to produce different climate impacts not only from the single-year events but also between the first and second austral winters of the multi-year events, both of which are the focus of the present study.

There have only been six multi-year events during the past four decades (1979–2020). The small sample size makes it difficult to robustly identify the possible different climate impacts of multi-year La Niña events. We address this issue in the present study by utilizing the 2,200-year Pre-Industrial simulation produced by NCAR's Community Earth System Model version 1 (CESM1; Kay et al., 2015). This particular CESM1 simulation has been shown to produce reasonably good simulations of single and multi-year El Niño and La Niña events, whose properties are reasonably realistical in terms of the spatial patterns and temporal evolutions of the associated sea surface temperature anomalies (SSTAs) as well as their inter-basin interactions with the neighboring Atlantic and Indian oceans (Kim and Yu, 2020, 2021, 2022). Therefore, it is useful to use the large number of multi-year events provided by this CESM1 simulation to first identify and examine the climate impacts of multi-year La Niñas and then verify the model findings with observed events. Section 2 gives details about data and methods. The model results and the observational verification are presented in Section 3. Section 4 concludes with the findings and implications of the study.

2. Data and Methods

We analyze the monthly anomalies of geopotential height, sea level pressure (SLP), sea surface temperature (SST), surface air temperature (SAT), wind, and SIC from years 400–2200 of the 2,200-year CESM1 Pre-Industrial Control simulation. We use the observations and reanalyses during period 1979–2020 to verify the model findings. These data include the monthly SIC and SST data from the Hadley Center Sea Ice and SST (HadlSST; Rayner et al., 2003) and monthly geopotential height, SLP, and SAT data from the NCEP-DOE Reanalysis II data (Kanamitsu et al., 2002). 1979 to 2020 is the period when satellite remote sensing was available to provide more reliable Antarctic and sea ice observations. In this study, monthly anomalies are defined as the deviations from the monthly climatology after the linear trend is removed. The modeled and observed monthly climatologies are calculated as the means during years 400–2200 of the CESM1 simulation and the years 1979–2020 of the observations and reanalysis, respectively.

We identified a La Niña event to occur in the CESM1 simulation or the reanalysis when the 3-month running-mean of the Ocean Niño index (ONI; SST anomalies averaged between 5°S–5°N and 170°W–120°W) is less than −0.75 standard deviation at any time during November^{0} to January^{+1}. Here, the year before the onset of the La Niña is referred to as year −1, while the onset year and the first and second years after the onset year are referred to as years 0, +1, and +2, respectively. Calendar months during those years are referred to as month^{-1}, month^{0}, month^{+1}, and month^{+2}, respectively. Following Kim and Yu (2022), if the running-mean ONI during any month from November^{+1} to January^{+2} of the selected events is less than 0°C, the event is classified as a multi-year La Niña event. Otherwise, the event is classified as a single-year La Niña event. Three other SSTA indices were also used in the study (see Text S1 in Supporting Information S1), which include the IOD index, zonal location (ZL) index, and tropical north Atlantic (TNA) index.

A two-tail student *T* test is used to examine the statistical significance of composite and regression analysis results.

3. Results

3.1. SSTA Characteristics During Single- and Multi-Year La Niñas

During years 400–2,200 of the CESM1 simulation, there are a total of 351 La Niña events, 252 of which (72%) are multi-year events and 99 of which (28%) are single-year events. The relative percentages of single and multi-year

La Niña events in the simulation are close to the percentages (i.e., 75% and 25% respectively) observed during the analysis period 1979–2020, when six multi-year La Niña events and two single-year La Niña events occurred. The ONI standard deviation during the DJF season of the La Niña events is 1.13°C in the CESM1 simulation and 1.14°C in the reanalysis, which indicate that the simulated and observed La Niña events have comparable peak intensities. The composite SSTA evolution indicates that the simulated single-year La Niña typically starts to develop in MAM^{0}, intensifies during JJA^{0} and September-October-November (SON^{0}), peaks during DJF^{0}, decays during MAM^{+1}, and transitions to El Nino during JJA^{+1} (Figure S1a in Supporting Information S1). During the developing austral winter (JJA^{0}), the composite SSTAs are centered over the tropical Eastern Pacific (EP) and display an EP type of pattern (Figures S1a and S1b in Supporting Information S1). The event is accompanied by a negative IOD, which peaks during SON^{0} of the developing year (Figures S1a and S1b in Supporting Information S1). The composite index values during the JJA^{0} season (Figure S1c in Supporting Information S1) further confirm that the single-year La Niña is of the EP type of SSTA pattern (the ZL index is negative), accompanied by a negative phase of the IOD and weak SSTAs in the TNA. It should be noted that the North Atlantic La Niña-induced SSTAs become stronger with negative values during MAM^{+1} (see Figure S1a in Supporting Information S1).

For the simulated multi-year La Niña events, their composite negative SSTAs (Figure 1a) onset in MAM^{0} and persist into MAM^{+2} with the second DJF^{+1} peak value weaker than the first DJF^{0} peak value. The composite SSTAs during the simulated multi-year La Niña events show three key differences from the composite SSTAs during the simulated single-year La Niñas. The first key difference appears in their pre-onset Pacific SSTAs. The composite multi-year La Niña is preceded by SSTAs characteristic of a strong El Niño that are absent from the single-year composite La Niña (cf., Figure 1a and Figure S1a in Supporting Information S1). Several previous studies have emphasized this pre-onset strong El Niño condition to explain the generation of multi-year La Niña events (Iwakiri & Watanabe, 2021; Larson & Pegion, 2020).

The second key difference appears in the La Niña-induced SST anomalies in the neighboring Atlantic and Indian Oceans. The negative SSTAs typically induced by La Niña in the neighboring Atlantic and Indian Oceans (Alexander et al., 2002; Enfield & Mayer, 1997; He et al., 2020; Klein et al., 1999; Schott et al., 2009) appear in the composite simulated single-year La Niña (Figure S1a in Supporting Information S1). However, these typical cross-basin impacts of La Niñas appear only during the second austral winter in the multi-year La Niña composite (see JJA^{+1} in Figures 1a and 1c) but are absent during its first developing year (see JJA^{0} in Figures 1a and 1b). This key difference is related to the first key difference in the pre-onset Pacific SSTAs. Figure 1a indicates that the preceding El Niño before the onset of the multi-year La Niña induces a basin-wide warming in the Indian Ocean that lasts into the onset year (i.e., year 0) of the multi-year La Niña. It is evident from Figure 1b that the positive IOD pattern characteristic of El Niño is still present in the first austral winter (JJA^{0}) of the event, even though the La Niña has developed into large intensity in the Pacific. The lagged warming cancels out the negative IOD typically induced by the La Niña. This residual effect from the pre-onset El Nino condition explains why the multi-year La Niña does not produce a negative IOD during its first year. During the second year of a multi-year La Niña, the negative IOD appears (Figures 1a and 1c). These contrasting IOD conditions between the first and second years of the multi-year La Niña is reflected clearly in the value of the IOD index (Figure 1d), which has a small positive value during the first austral winter (JJA^{0}) but a large negative value during the second austral winter (JJA^{+1}). The pre-onset El Niño condition also induces warm SSTAs over the tropical Atlantic that persist into the first year of the multi-year La Niña (Figure 1b). These warm SSTAs are replaced by cold SSTAs during the second year of the event (Figure 1c) and the TNA index changes from a positive value in JJA^{0} to a negative value in JJA^{+1} (Figure 1d).

The third key difference between the single and multi-year La Niñas appears in the SSTA characteristics within the tropical Pacific. The largest SSTAs during single-year La Niñas are located in the tropical eastern-to-central Pacific during the developing year (see Figure S1a in Supporting Information S1). For the JJA season specifically, the single-year La Niña is of the EP type (Figure S1b in Supporting Information S1) and is characterized by negative values of the ZL index (Figure S1c in Supporting Information S1). During the multi-year La Niñas the largest SSTAs are located in the tropical eastern-to-central Pacific during the first year but more in the tropical Central Pacific (CP) during the second year (see Figure 1a). For the JJA season specifically, the multi-year La Niña is of the EP type during the first austral winter with a larger intensity (Figure 1b) but of the CP type (Kao & Yu, 2009; Yu & Kao, 2007) with a smaller intensity during the second austral winter (Figure 1c). This location

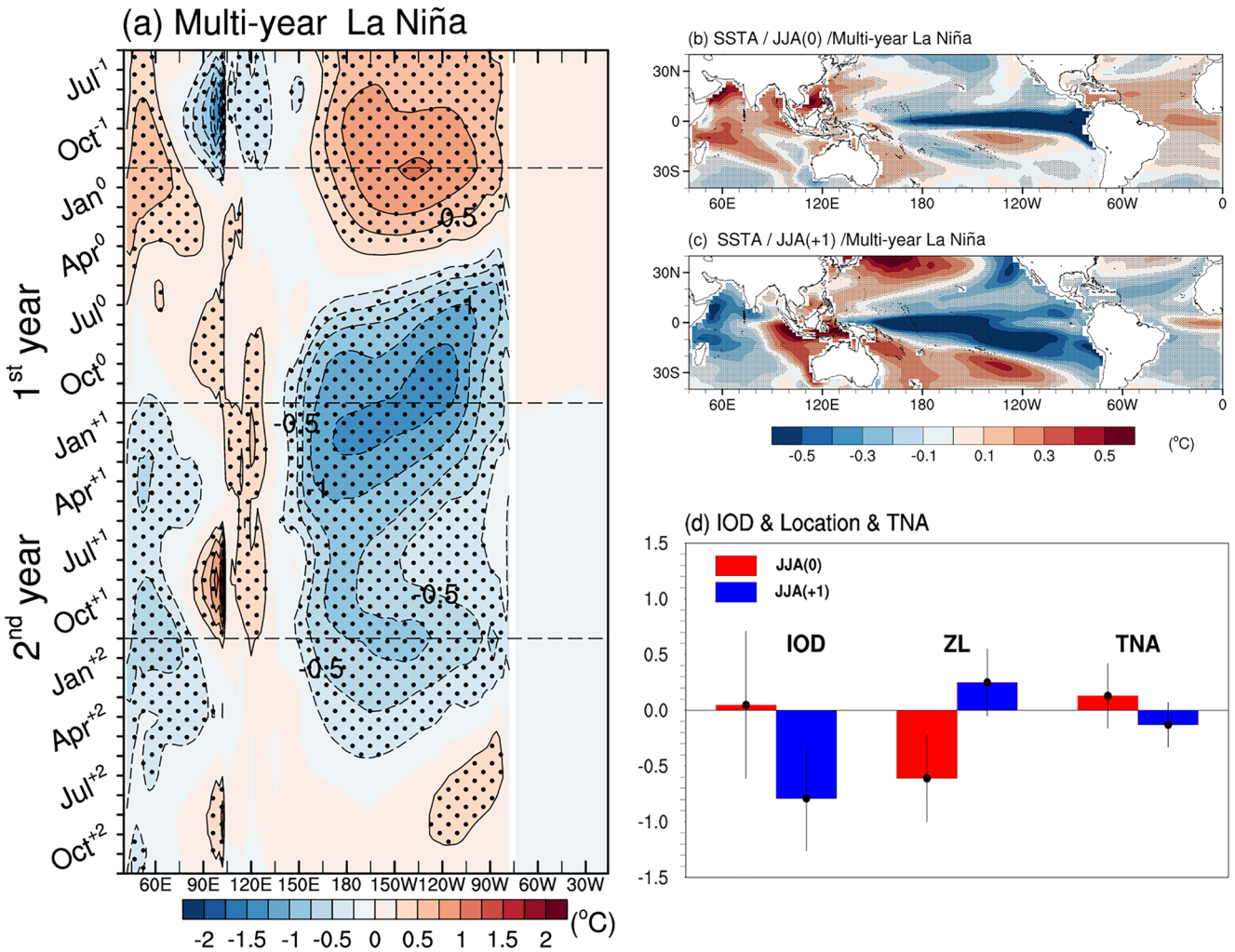

Figure 1. Composite SSTAs of the multi-year La Niñas simulated during years 400–2,200 of the CESM1 Pre-industrial simulation: (a) longitude–time plot of equatorial (5°S–5°N) Pacific SSTAs (shaded; in °C) from June^{-1} to December^{+2}; (b) composite SSTA pattern during the first austral winter (JJA0) of the events; (c) composite SSTA pattern during the second austral winter (JJA^{+1}); and (d) values of the composite IOD, ZL, and TNA indexes during the JJA^{0} (red bars) and JJA^{+1} (blue bars). Dots indicate areas where the values exceed the 95% confidence interval determined using a two-tailed Student's *t* test.

shift is reflected in the value of the ZL index, which changes from a negative value during first austral winter (JJA^{0}) to a positive value during the second austral winter (JJA^{+1}).

In brief, the unique pre-onset Pacific conditions cause multi-year La Niñas to have different teleconnections over the tropical Indian and Atlantic Oceans during their first austral winter than single-year La Niñas. The differences disappear during the second austral winter. We next examine whether these differences can cause the multi-year La Niña to produce different impacts than the single-year La Niña on Antarctic SICs during austral winter (i.e., JJA).

3.2. Impacts of the Multi-Year La Niña on Antarctic Sea Ice Concentrations

We compare in Figure 2 the SIC anomaly patterns composited for the single and multi-year types of simulated La Niña events during austral winter. The single-year La Niña in the CESM1 induces a tripolar pattern of SIC anomalies in the vicinity of Antarctica with one major negative anomaly center over the Weddell-Bellingham Sea and two positive anomaly centers over the Amundsen-Ross Sea and the African sector (between 30°W and 30°E) of the Southern Ocean (Figure 2c). This tripolar pattern includes in it the so-called Antarctic Dipole pattern that Yuan (2004) identified to describe the typical ENSO impacts on Antarctic SIC. Our composite

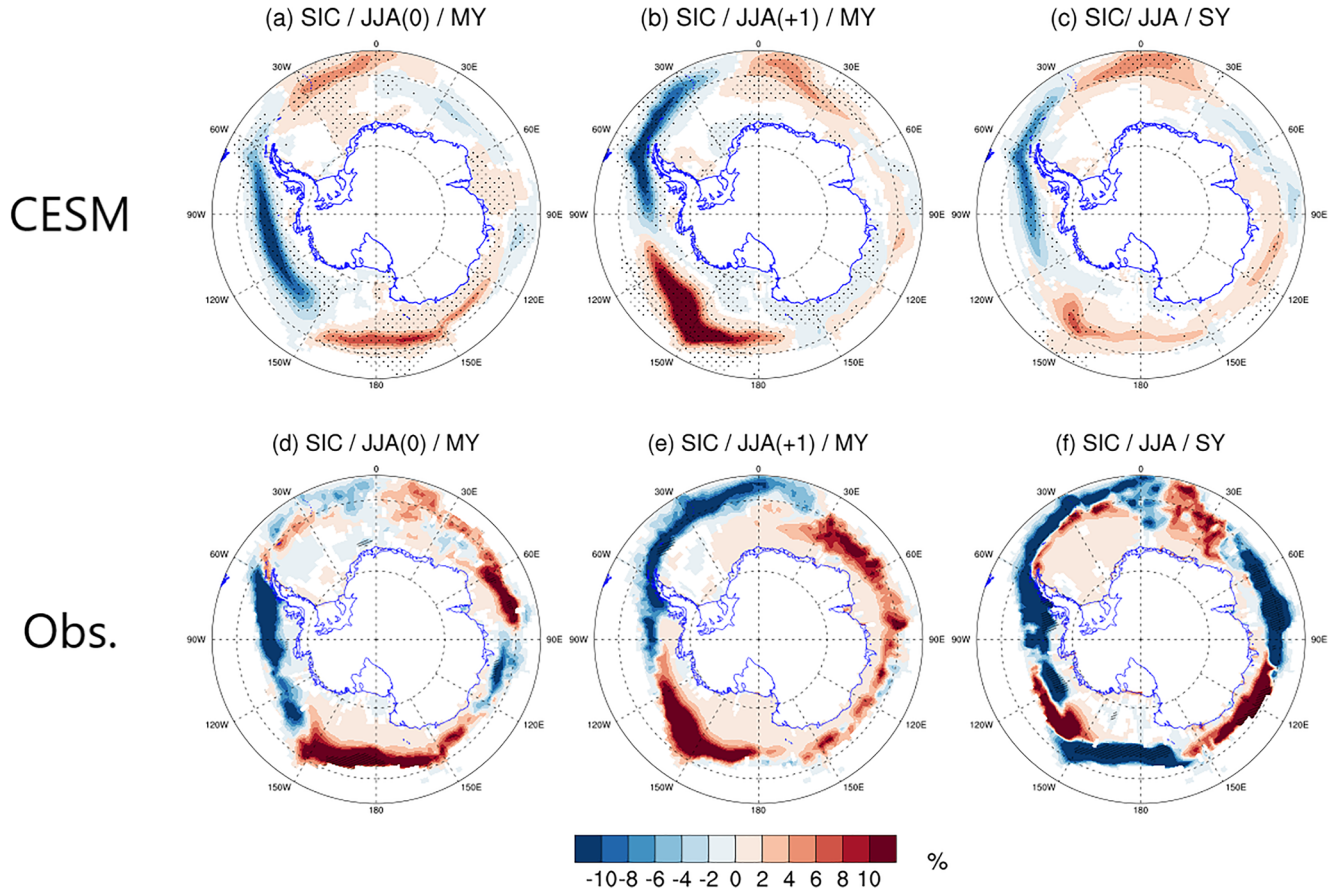

Figure 2. Sea ice concentration (SIC) anomalies composited for the (a) first austral winter (JJA^0) and (b) second austral winter (JJA^{+1}) of the simulated multi-year La Niña events and (c) the austral winter (JJA^0) of the simulated single-year La Niña events in the CESM1 simulation. (d–f) are the same as (a–c) but calculated using the observed La Niña events during the period 1979–2020. Dots in (a–c) indicate areas where the values exceed the 95% confidence interval determined using a two-tailed Student's *t* test. Significance tests were not applied to the observed composites in (d–f) due to small sample sizes.

result indicates that the CESM1 can realistically simulate the observed impact of single-year La Niña events on Antarctic SIC. A similar tripolar SIC pattern appears during the second austral winter of the multi-year La Niña events (Figure 2b). However, during the first austral winter, the tripolar pattern is shifted westward by about 30° with the three anomaly centers moved to the Weddell Sea, the Bellingshausen-Amundsen Sea, and the Ross Sea (Figure 2a). This zonal shifting of the SIC anomaly pattern is an interesting feature of multi-year La Niña events and indicates that it is the first austral winter of the multi-year events that produces a different impact on Antarctic climate from the single-year La Niña. A similar zonal shifting of the tripolar SIC anomaly pattern between the first and second austral winters can be found in the composites of the observed multi-year La Niña events during the period 1979–2020 (Figures 2d and 2e). The composite SIC anomaly pattern for the observed single-year La Niña (Figure 2f) also verify the similarity between the impacts produced by single-year La Niñas and the second winter of multi-year La Niñas. It is impressive to see that the SIC anomaly patterns produced by the CESM1 for the single and multi-year La Niñas are so similar to those observed. We further analyzed the long-term CESM1 simulation to uncover the cause of the zonal-shifted Antarctic SIC impacts during the first winter of multi-year La Niñas.

3.3. The Physical Mechanisms Behind the Shifting Tripolar SIC Patterns

To explore the physical mechanisms, we examined the composite SAT and SLP anomalies during the two JJA seasons of multi-year La Niñas. We find the negative (positive) SIC anomaly centers to be overlaid with warm (cold) SAT anomaly centers (cf. Figures S2a, S2b, S2e, and S2f in Supporting Information S1). The overlapping suggests that the tripolar SIC anomaly pattern is thermally driven by SAT variations. When the SAT anomaly

pattern shifts from one austral winter to the other, the SIC anomaly pattern shifts accordingly. The composite SLP analysis (Figures S2i–S2j in Supporting Information S1) further suggests that the SAT variations are a result of thermal advection driven by the SLP anomalies. The warm SAT anomaly center over the Bellingshausen-Weddell Sea and the cold SAT anomaly center over the Amundsen-Ross Sea during the second austral winter are respectively located to the east and west of a negative SLP anomaly center over the Amundsen Sea (Figure S2j in Supporting Information S1). The SLP anomaly center induces an anomalous cyclonic circulation that transports warmer air on its eastern side from middle latitudes toward the Antarctic to produce the warm SAT anomaly center and transports colder air on its western side out of the Antarctica to produce the cold SAT anomaly center (see the surface wind vectors shown in Figures S2f and S2j in Supporting Information S1). The westward-shifted tripolar SIC pattern during the first winter can also be explained as a result of the SAT thermal forcing (Figure S2e in Supporting Information S1) induced by SLP anomalies (Figure S2i in Supporting Information S1). However, the negative SLP anomaly center during the first winter is located westward of that during the second winter. The surface anomalous cyclone located over the Amundsen Sea during the second austral winter but over the Ross Sea during the first austral winter. Consistent differences can also be found among other centers of SIC, SAT, and SLP anomalies (Figures S2a, S2b, S2e, S2f, S2i, and S2j in Supporting Information S1) between the first and second winters. It can be concluded that the zonal shifting feature of the tripolar SIC anomaly pattern between the first and second austral winters of the multi-year La Niña is caused by corresponding shifts in the SLP anomaly centers.

The major SLP anomaly centers responsible for shaping the SIC anomaly patterns appear to be components of wave trains that emanate from the tropics (Figures S2i and S2j in Supporting Information S1). The wave train patterns are very apparent in the composite 500-hPa geopotential height (Z500) anomalies (Figures 3a and 3b). Major Z500 anomaly centers overlap with the SLP anomaly centers indicating that these wave trains have a barotropic structure (cf. Figures 3a–3b and Figure S2i–S2j in Supporting Information S1). As previously mentioned, the multi-year La Niña exhibits different SSTA characteristics between its first and second austral winters, including the location of primary SSTAs in the tropical Pacific and their induced IOD and TNA SST anomalies. To find out how these differences contribute to the different wave train patterns between the two winters, we separately regressed the Z500 anomalies onto the reversed values of the IOD, ZL, and TNA indices (Figures 3d–3f). We find that the Z500 composite difference pattern between the two austral winters (Figure 3c) has a centered pattern correlation of 0.87 with the IOD-regressed pattern, 0.45 with the TNA-regressed pattern, and only 0.03 with the ZL-regressed pattern. Thus, it is the IOD-regression pattern (Figure 3d) that causes the Z500 anomaly pattern to be different between the first and second austral winters of the multi-year La Niña. At middle and high latitudes of the Southern Hemisphere, the Z500 difference pattern in Figure 3c has three positive centers between the 45°S and 60°S latitude circles (centers "A" at 30°W, "B" at 180°E, and "C" at 70°E) and two negative centers south of 60°S latitude (centers "D" at 100°W and "E" over the Antarctic Continent). The locations of these difference centers match well with the Z500 anomaly centers in the IOD-regression pattern (cf. Figures 3c and 3d). This result indicates that different IOD conditions between the two austral winters (i.e., a weak positive IOD during the first austral winters and a strong negative IOD during the second austral winter) are most responsible for producing the zonal shift in the tripolar SIC anomaly pattern during multi-year La Niña events. The different TNA conditions (Figure 3f) between the two austral winters have some contribution to the circulation (i.e., Z500 and SLP) differences in the vicinity of Centers B–D, while the different ZL locations contribute more to the circulation differences near Center C.

How do the IOD SSTAs excite the Z500 anomaly pattern shown in Figure 3d? To answer this question, we compare the IOD-regressed Z500 anomaly pattern to the leading modes of variability in the austral winter Z500 anomalies. The first three leading modes identified by applying an Empirical Orthogonal Function (EOF) analysis to the simulated JJA Z500 anomalies are the Southern Annual Mode (SAM; Figure 3g), Pacific South America 1 (PSA1) mode (Figure 3h), and Pacific South America 2 (PSA2) mode (Figure 3i). Based on the locations of the major anomaly centers, we can see that the IOD regression pattern is comprised of both the SAM and PSA1 patterns. Both the SAM and PSA1 modes have large anomalies near Centers A–E of the IOD-repressed pattern. The IOD-regressed anomaly pattern is correlated most highly (0.94) in mid and high latitudes with the PSA1 mode, the second highest correlation (0.67) is with the SAM mode, and the lowest correlation (0.14) is with the PSA2 modes. It is apparent that the different IOD conditions enable the multi-year La Niña to produce different PSA1 and SAM modes in its first and second austral winters, giving rise to a zonally-shifted SIC tripolar anomaly pattern during the lifecycle of multi-year La Niñas.

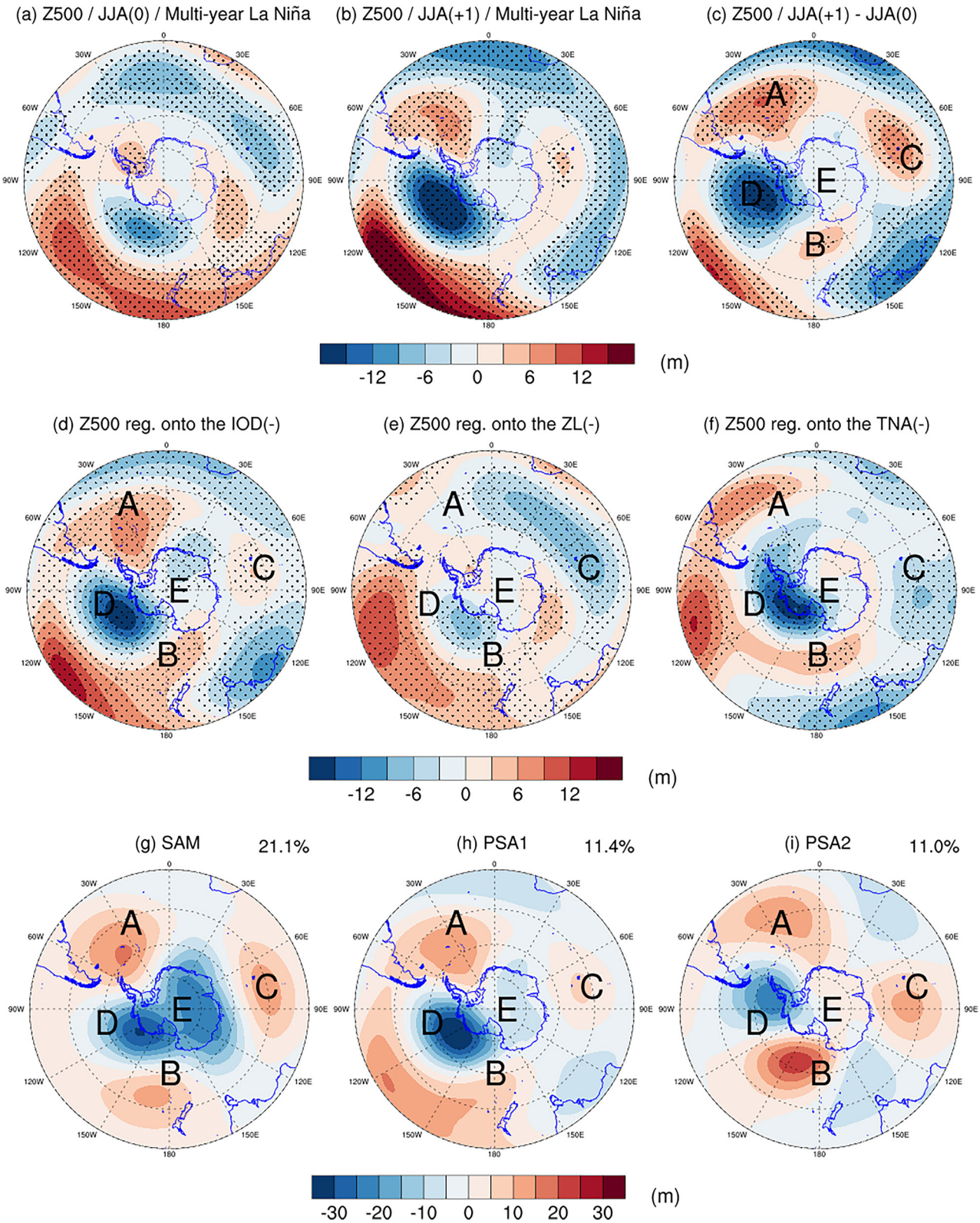

Figure 3. Composite 500 hPa geopotential height (Z500) anomalies during the (a) first austral winter (JJA0) and (b) second austral winter (JJA+1) of the simulated multi-year La Niñas and (c) their differences (JJA+1 minus JJA0). Z500 anomalies regressed onto the (d) negative IOD index, (e) negative ZL index, and (f) negative TNA index during the June-July-August season. The three leading EOF modes (i.e., (g) SAM, (h) PSA1, and (i) PSA2) of Z500 anomalies during the June-July-August season. Results are calculated using years 400–2,200 of the CESM1 Pre-Industrial simulation. Dots indicate areas where the values exceed the 95% confidence interval determined using a two-tailed Student's *t* test. Centers A–E are explained in the main text.

3.4. The Shifting SIC Anomaly Patterns During Observed Multi-Year La Niña Events

To verify the shifting SIC impact, and the impact mechanism, found in the CESM1's multi-year La Niñas, we performed the same composite analyses for the single and multi-year La Niñas observed during the period 1979–2020. There are two single-year events (2005–2006 and 2017–2018) and six multi-year events (1983–1985, 1988–1990, 1995–1997, 1998–2000, 2007–2009, and 2010–2012) during the period. The composite analyses with SSTAs confirm that, similar to the simulated events, the observed multi-year events are preceded by a strong El Nino condition before onset (Figure S3a in Supporting Information S1), accompanied by a positive IOD during the first austral winter (Figure S3b in Supporting Information S1) but a negative IOD during the second austral winter (Figure S3c in Supporting Information S1), and the zonal locations of the primary tropical Pacific SSTAs differ between the two winters (Figures S3a–S3c in Supporting Information S1). The values of the IOD, TNA, and ZL indices (Figure S3d in Supporting Information S1) quantify these three key differences in the characteristics of the SSTAs between the two austral winters of the observed multi-year La Niña. As for the observed single-year La Niñas, their composite SSTA evolution and characteristics (Figure S4 in Supporting Information S1) are similar to what have been described for the simulated single-year La Niñas (cf., Figure S1 in Supporting Information S1), although minor differences exist in its teleconnections to the IOD and TNA.

Despite the small sample sizes, the observed single and multi-year event composites show SIC anomaly patterns (Figures 2d–2f) that are similar to the CESM1-simulated ones. Since there are only two observed single-year events, the pattern of the composited SIC anomalies are not as smooth as the CESM1-simulated one. Nevertheless, similar to the simulated composite, negative SIC anomalies occur over the Weddle-Bellingham Sea and positive anomalies occur over the Amundsen Sea in the observations (cf. Figures 2f and 2c). The observed composite is most different form the simulated composite over the Ross Sea area. The observed composite for the multi-year La Niña shows a tripolar pattern of SIC anomalies that shifts eastward from the first to second austral winters (Figures 2d and 2e), and the observed SIC anomaly pattern during the second austral winter also resembles the observed single-year La Niña composite pattern (Figure 2f). The anomaly centers of the observed and simulated tripolar patterns coincide reasonably well with each other for both the first and second austral winters (cf., Figures 2a and 2b and 2d-2e; also reproduced in Figures S2a–S2d in Supporting Information S1). Similar to what we found from the CESM1 simulation, the observed SIC impacts are thermally driven by SAT anomalies (Figures S2g and S2h in Supporting Information S1), whose major anomaly centers overlay directly over the SIC anomaly centers. The observed SAT anomalies can also be explained as a result of meridional temperature advection induced by the SLP responses to the multi-year La Niña (Figure S2k and S2l in Supporting Information S1).

To make sure that the shifting tripolar pattern in the observed composites is not an artifact of a particular multi-year La Niña event, we compare the SIC anomalies during the first and second winters of every one of the six multi-year La Niña events (Figure S5 in Supporting Information S1). The shifting tripolar pattern can be found in four (the 1988–1990, 1995–1997, 1998–2000, and 2007–2009 events) of the six events. Thus, the zonal-shifting impacts of the multi-year La Niña on Antarctic SIC and the impact mechanism identified from the long-term CESM1 simulation can be verified by the observed events. This indicates that the shifting tripolar pattern is a robust feature of the impact of multi-year La Niñas on Antarctic SICs and that the CESM1 is capable of faithfully reproducing this impact and La Niña's teleconnections to the Southern hemispheric atmospheric circulation.

4. Concluding Remarks

In this study, we used the large number of La Niña events produced in a 2,200 years CESM1 simulation to reveal a distinct zonally shifting impact of the multi-year La Niña on Antarctic SIC. In addition, the mechanisms for this austral winter impact were uncovered. The identified impact and impact mechanism were then verified using observed La Niña events during the period 1979–2020. The distinct impact occurs only during the first austral winter of the multi-year La Niña. The unique SIC impact is a result of the unique pre-onset El Niño conditions that are often found to occur before multi-year La Niña events. The teleconnections forced by the pre-onset El Niño over the Indian Ocean lasts into the first winter of multi-year La Niñas to excite a different wave train into the southern hemisphere to give rise to the distinct SIC anomaly pattern. Our findings demonstrate that the pre-onset condition is not only important to the underlying dynamics of the multi-year La Niña but also in shaping the climate impacts of the multi-year La Niña. Our findings also suggest that it is important to be able to classify

and predict the evolution of La Niña events to more accurately prepare for the climate impact it may produce in the Antarctic.

Data Availability Statement

The 2200-yr CESM1 Pre-Industrial Control simulation can be accessed from Earth System Grid (https://www.cesm.ucar.edu/projects/community-projects/LENS/data-sets.html). The observed SIC data comes from the Met Office Hadley Center (https://www.metoffice.gov.uk/hadobs/hadisst/data/download.html). The Reanalysis II data are available from this website (https://psl.noaa.gov/data/gridded/data.ncep.reanalysis2.html).

Acknowledgments
We thank two anonymous reviewers for their valuable comments. This research is supported by NSF Climate and Large-Scale Dynamics Program under Grant AGS-2109539. The authors are grateful to all data providers.

References

Alexander, M. A., Bladé, I., Newman, M., Lanzante, J. R., Lau, N. C., & Scott, J. D. (2002). The atmospheric bridge: The influence of ENSO teleconnections on air–sea interaction over the global oceans. *Journal of Climate*, *15*(16), 2205–2231. https://doi.org/10.1175/1520-0442(2002)015<2205:tabtio>2.0.co;2

Enfield, D. B., & Mayer, D. A. (1997). Tropical Atlantic sea surface temperature variability and its relation to El Niño-Southern Oscillation. *Journal of Geophysical Research*, *102*(C1), 929–945. https://doi.org/10.1029/96jc03296

He, S., Yu, J. Y., Yang, S., & Fang, S. W. (2020). ENSO's impacts on the tropical Indian and Atlantic Oceans via tropical atmospheric processes: Observations versus CMIP5 simulations. *Climate Dynamics*, *54*(11), 4627–4640. https://doi.org/10.1007/s00382-020-05247-w

Hu, Z. Z., Kumar, A., Xue, Y., & Jha, B. (2014). Why were some La Niñas followed by another La Niña? *Climate Dynamics*, *42*(3–4), 1029–1042. https://doi.org/10.1007/s00382-013-1917-3

Iwakiri, T., & Watanabe, M. (2020). Multiyear La Niña impact on summer temperature over Japan. *Journal of the Meteorological Society of Japan. Ser. II*, *98*(6), 1245–1260. https://doi.org/10.2151/jmsj.2020-064

Iwakiri, T., & Watanabe, M. (2021). Mechanisms linking multi-year La Niña with preceding strong El Niño. *Scientific Reports*, *11*(1), 1–11. https://doi.org/10.1038/s41598-021-96056-6

Kanamitsu, M., Ebisuzaki, W., Woollen, J., Yang, S. K., Hnilo, J. J., Fiorino, M., & Potter, G. L. (2002). NCEP–DOE AMIP-II reanalysis (r-2). *Bulletin of the American Meteorological Society*, *83*(11), 1631–1644. https://doi.org/10.1175/bams-83-11-1631(2002)083<1631:nar>2.3.co;2

Kao, H. Y., & Yu, J. Y. (2009). Contrasting eastern-Pacific and central-Pacific types of ENSO. *Journal of Climate*, *22*(3), 615–632. https://doi.org/10.1175/2008jcli2309.1

Kay, J. E., Deser, C., Phillips, A., Mai, A., Hannay, C., Strand, G., et al. (2015). The Community Earth System Model (CESM) large ensemble project: A community resource for studying climate change in the presence of internal climate variability. *Bulletin of the American Meteorological Society*, *96*(8), 1333–1349. https://doi.org/10.1175/bams-d-13-00255.1

Kim, J. W., & Yu, J. Y. (2022). Single- and multi-year ENSO events controlled by pantropical climate interactions. *NPJ Climate and Atmospheric Science*, *5*(1), 88. https://doi.org/10.1038/s41612-022-00305-y

Kim, J. W., & Yu, J. Y. (2020). Understanding reintensified multiyear El Niño events. *Geophysical Research Letters*, *47*(12), e2020GL087644. https://doi.org/10.1029/2020gl087644

Kim, J.-W., & Yu, J.-Y. (2021). Evolution of subtropical Pacific-onset El Nino: How its onset location controls its decay evolution. *Geophysical Research Letters*, *48*(5), e2020GL091345. https://doi.org/10.1029/2020GL091345

Klein, S. A., Soden, B. J., & Lau, N. C. (1999). Remote sea surface temperature variations during ENSO: Evidence for a tropical atmospheric bridge. *Journal of Climate*, *12*(4), 917–932. https://doi.org/10.1175/1520-0442(1999)012<0917:rsstvd>2.0.co;2

Larson, S. M., & Pegion, K. (2020). Do asymmetries in ENSO predictability arise from different recharged states? *Climate Dynamics*, *54*(3), 1507–1522. https://doi.org/10.1007/s00382-019-05069-5

Liu, J., Yuan, X., Rind, D., & Martinson, D. G. (2002). Mechanism study of the ENSO and southern high latitude climate teleconnections. *Geophysical Research Letters*, *29*(14), 24–31. https://doi.org/10.1029/2002gl015143

Nuncio, M., & Yuan, X. (2015). The influence of the Indian Ocean dipole on Antarctic sea ice. *Journal of Climate*, *28*(7), 2682–2690. https://doi.org/10.1175/jcli-d-14-00390.1

Okumura, Y. M., & Deser, C. (2010). Asymmetry in the duration of El Niño and La Niña. *Journal of Climate*, *23*(21), 5826–5843. https://doi.org/10.1175/2010JCLI3592.1

Okumura, Y. M., DiNezio, P., & Deser, C. (2017). Evolving impacts of multiyear La Niña events on atmospheric circulation and US drought. *Geophysical Research Letters*, *44*(22), 11–614. https://doi.org/10.1002/2017gl075034

Rayner, N. A. A., Parker, D. E., Horton, E. B., Folland, C. K., Alexander, L. V., Rowell, D. P., & Kaplan, A. (2003). Global analyses of sea surface temperature, sea ice, and night marine air temperature since the late nineteenth century. *Journal of Geophysical Research*, *108*(D14), 4407. https://doi.org/10.1029/2002jd002670

Schott, F. A., Xie, S. P., & McCreary, J. P., Jr. (2009). Indian Ocean circulation and climate variability. *Reviews of Geophysics*, *47*(1), RG1002. https://doi.org/10.1029/2007rg000245

Yu, J.-Y., & Kao, H.-Y. (2007). Decadal changes of ENSO persistence barrier in SST and ocean heat content indices: 1958-2001. *Journal of Geophysical Research*, *112*(D13), D13106. https://doi.org/10.1029/2006JD007654

Yuan, X. (2004). ENSO-Related impacts on Antarctic sea ice: A synthesis of phenomenon and mechanisms. *Antarctic Science*, *16*(4), 415–425. https://doi.org/10.1017/s0954102004002238

Yuan, X., Kaplan, M. R., & Cane, M. A. (2018). The interconnected global climate system—A review of tropical–polar teleconnections. *Journal of Climate*, *31*(15), 5765–5792. https://doi.org/10.1175/jcli-d-16-0637.1

References From the Supporting Information

Saji, N. H., Goswami, B. N., Vinayachandran, P. N., & Yamagata, T. (1999). A dipole mode in the tropical Indian Ocean. *Nature*, *401*(6751), 360–363. https://doi.org/10.1038/43854

Geophysical Research Letters

Supporting Information for

A shifting tripolar pattern of Antarctic sea ice concentration anomalies during multi-year La Niña events

Tingting Zhu[1] and Jin-Yi Yu[1]

[1]Department of Earth System Science, University of California, Irvine, CA, USA

Contents of this file

Text S1. Definitions of climate indices used in this study

Three indices based on sea surface temperature anomalies (SSTAs) in the tropics were used in the study. The IOD index (Saji et al. 1999) is defined as the SSTA difference between western Indian Ocean (50°-70°E, 10°S-10°N) and eastern Indian Ocean (90°E-110°E, 10°S-0°S). Following Kim and Yu (2022), a zonal location (ZL) index of El Niño-Southern Oscillation (ENSO) is defined as the difference between the SSTAs averaged over the tropical eastern Pacific (100°-160°W, 5°S-5°N) and the SSTAs averaged over the tropical central Pacific (150°E-160°W, 5°S-5°N). Positive ZL values indicate that the La Niña events are located more within the tropical central Pacific (CP) and are of the so-called CP type of ENSO (Yu and Kao 2007; Kao and Yu 2009), while negative values indicate the events are located more within the tropical eastern Pacific (EP) and are of the so-called EP type of ENSO. The tropical north Atlantic (TNA) index is defined as the SSTAs averaged between 15°-55°W and 5°-25°N.

Figure S1. Composite SSTAs (°C) for the single-year La Niñas occurring during years 400 to 2200 of the CESM1 Pre-industrial simulation: (a) longitude–time plot of equatorial (5°S–5°N) Pacific SSTAs (shaded; °C) from June^{-1} to December^{+2}; (b) composite SSTA pattern during JJA^{0}; and (c) values of the composite IOD, ZL and TNA indexes during JJA^{0}. Dots indicate areas where the values exceed the 95% confidence interval determined using a two-tailed Student's t test.

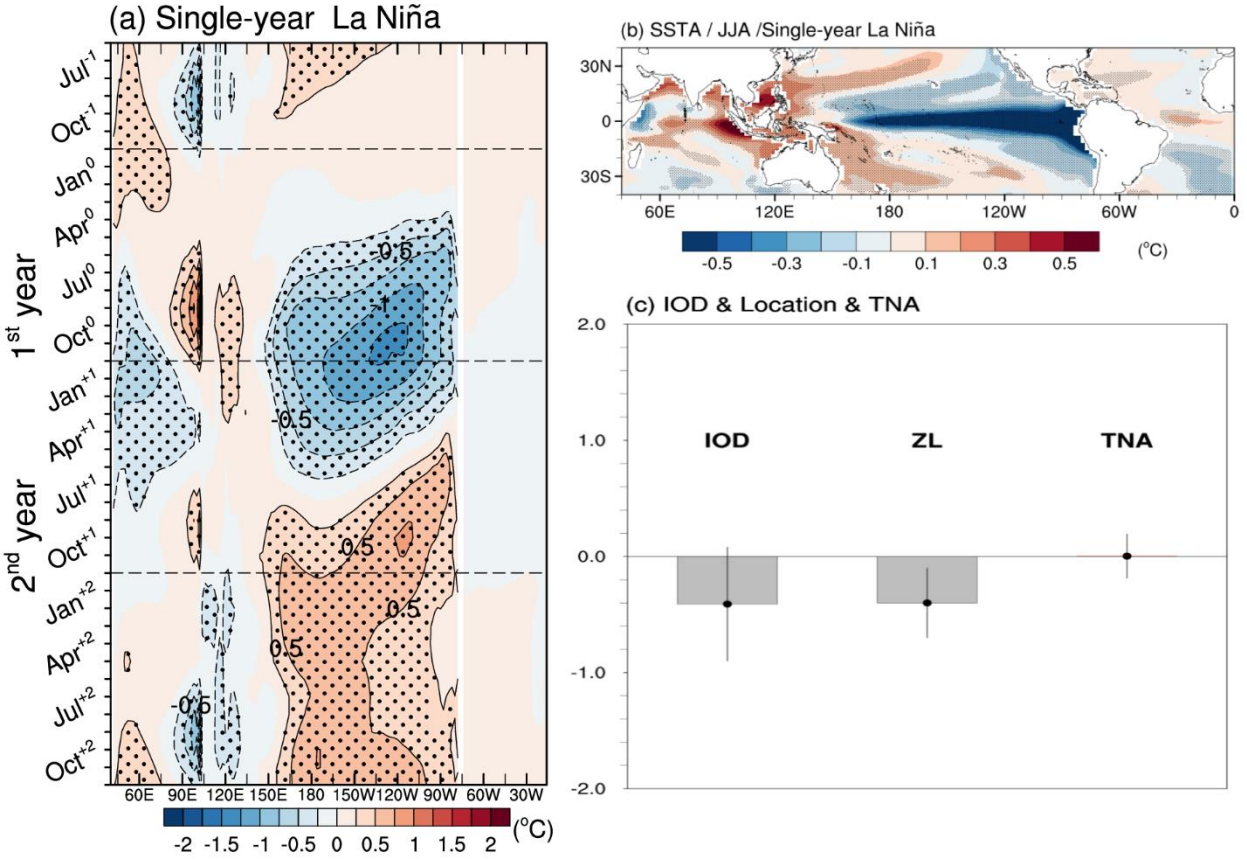

Figure S2. Composite anomalies in sea ice concentration (SIC; top panels), surface air temperature (SAT; °C, middle panels), and sea level pressure (SLP; hPa, bottom panels) for the simulated (left two columns of panels) and observed (right two columns of panels) multi-year La Niñas during the first austral winter (JJA^{0}; first and third-column panels) and second austral winter (JJA^{+1}; second and fourth-column panels). The simulated events are selected from years 400-2,200 of the CESM1 Pre-industrial simulation and the observed events are selected from the period 1979-2020. The outermost latitude circles in the top and middle panels are the 55° latitude, while it is the 30° latitude in the bottom panels. Composite surface wind vectors are superimposed in the middle and bottom panels. Dots indicate areas where the values exceed the 95% confidence interval determined using a two-tailed Student's t test.

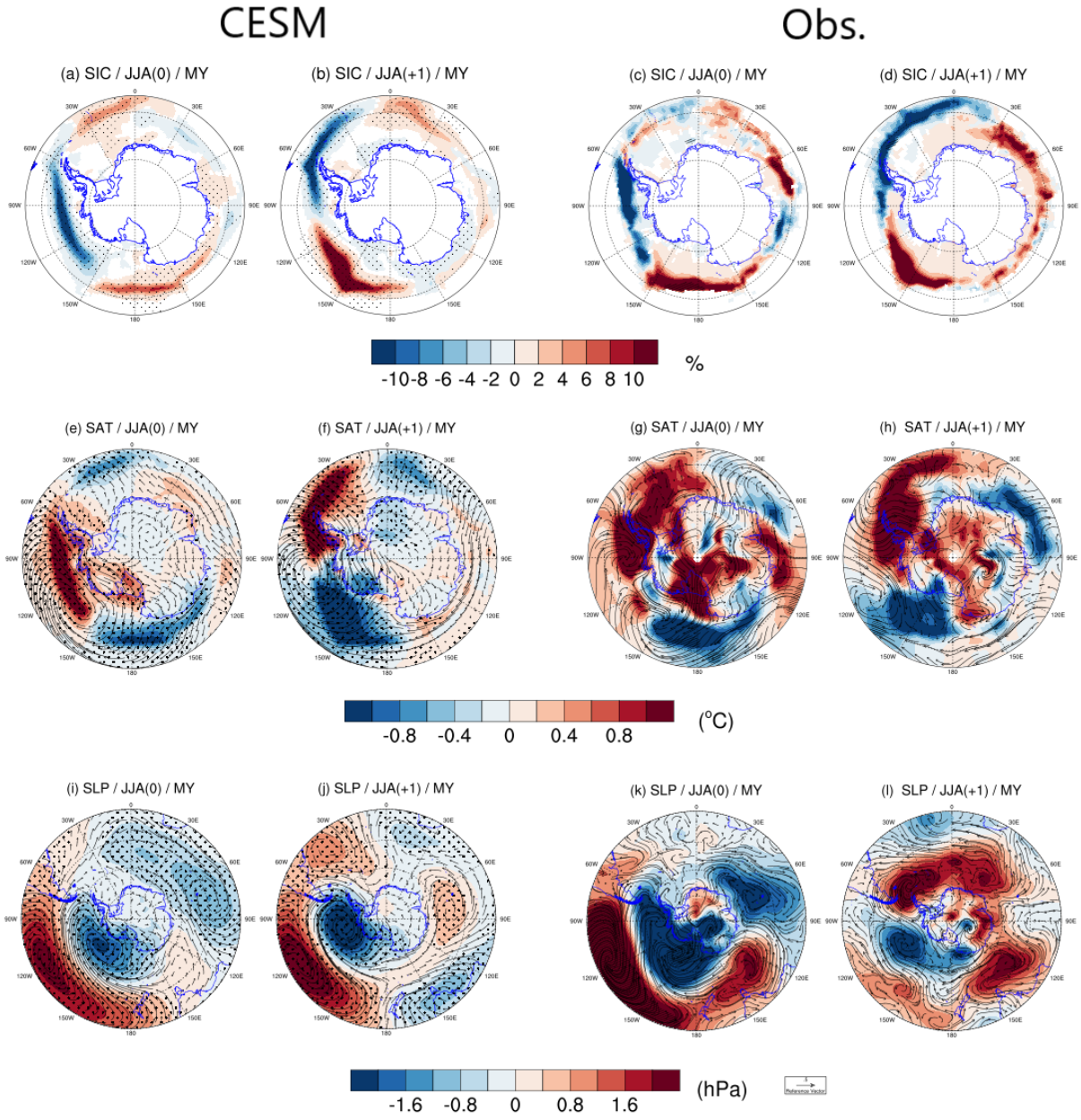

Figure S3. Composite characteristics of multi-year La Niñas observed during the period 1979-2020: (a) longitude–time plot of equatorial (5°S–5°N) Pacific SSTAs (shaded; °C) from June^{-1} to December^{+2}; (b) composite SSTA pattern during the first austral winter (JJA^{0}) of the vent; (c) composite SSTA pattern during the second austral winter (JJA^{+1}); and (d) values of the composite IOD, ZL and TNA indexes during the JJA^{0} (red bar) and JJA^{+1} (blue bar). Dots indicate areas where the values exceed the 95% confidence interval determined using a two-tailed Student's t test.

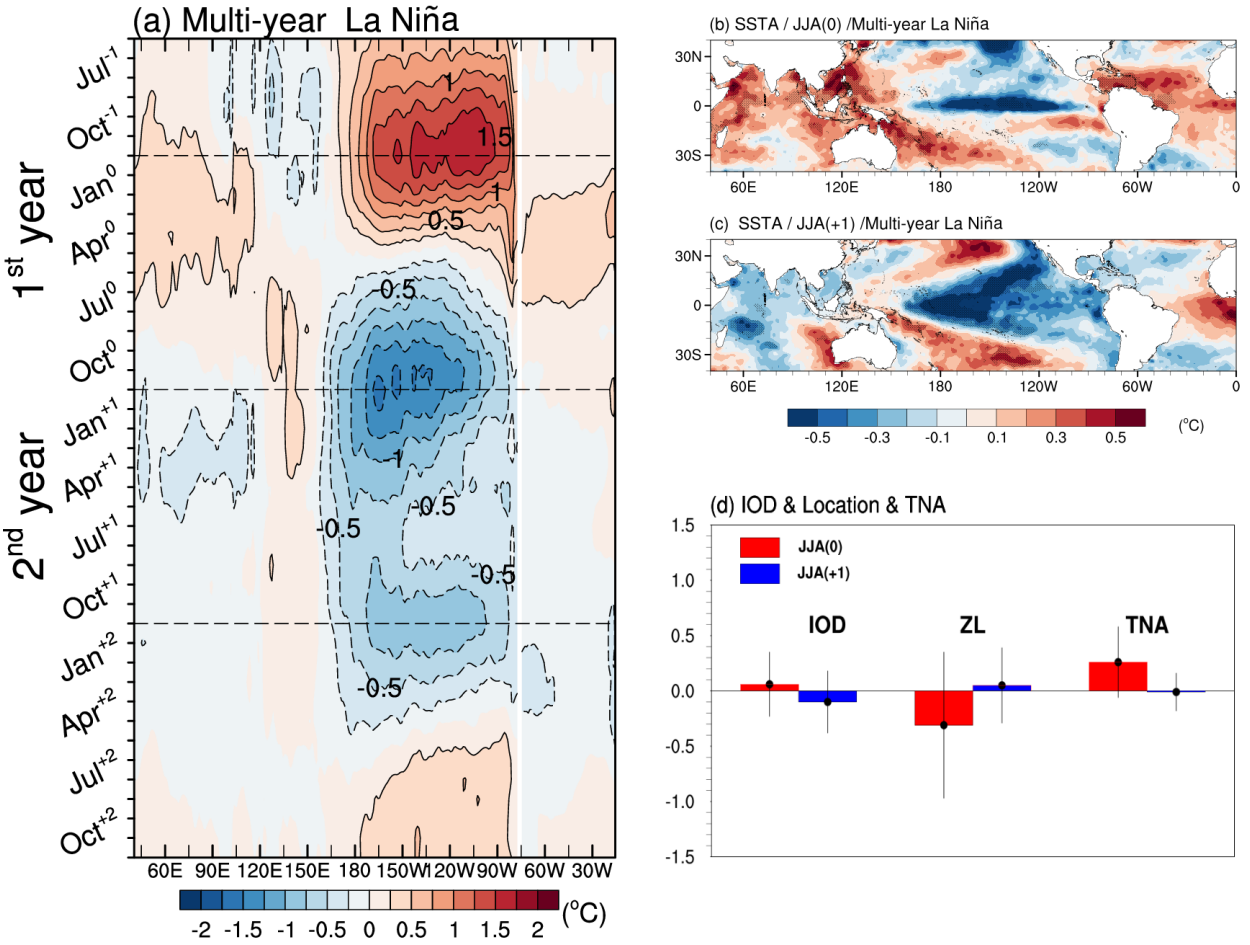

Figure S4. Same as Figure S3 but for the composite of observed single-year La Niña events.

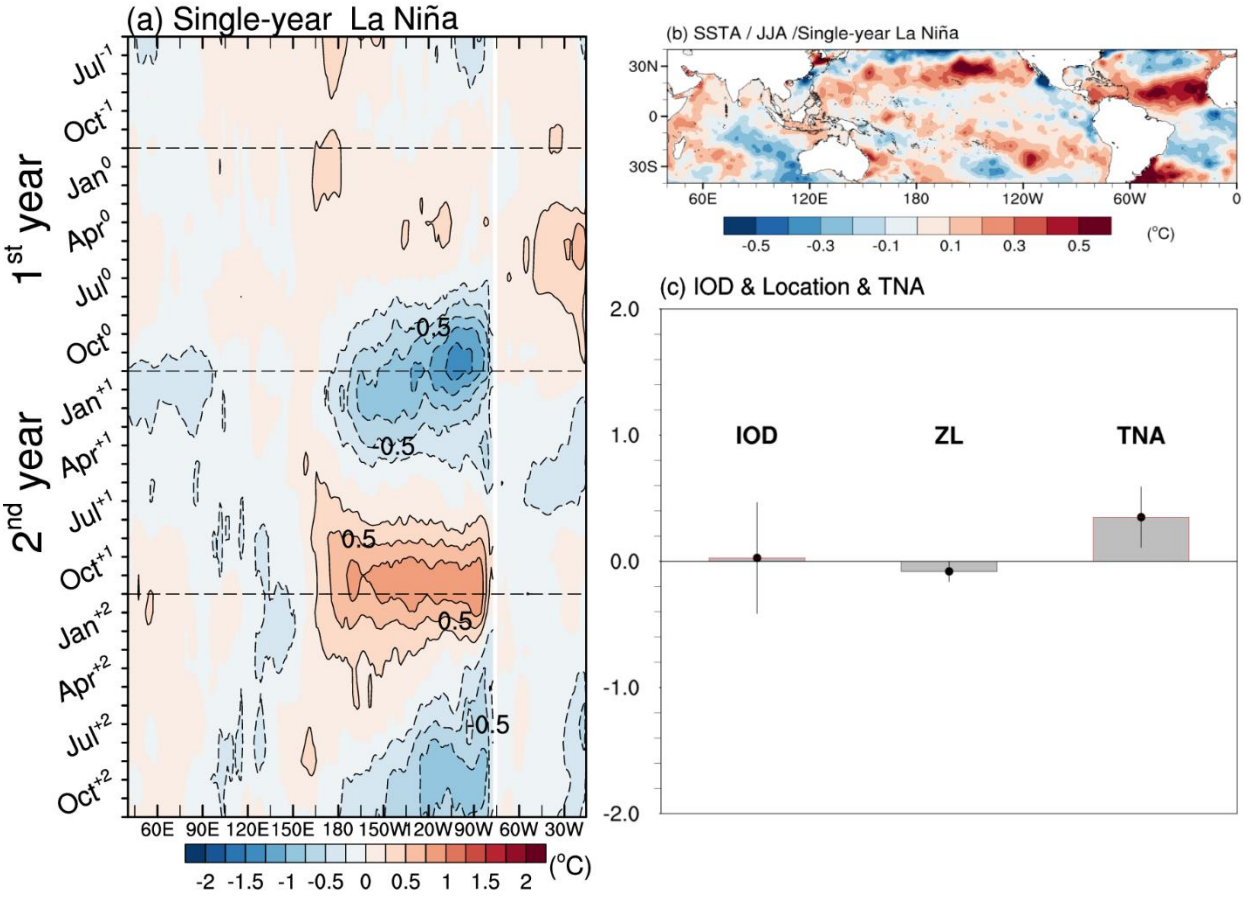

Figure S5. (a) The SIC anomalies during the first (JJA^{0}) and second (JJA^{+1}) austral winters of the six multi-year La Niña events observed during the period 1979-2020.

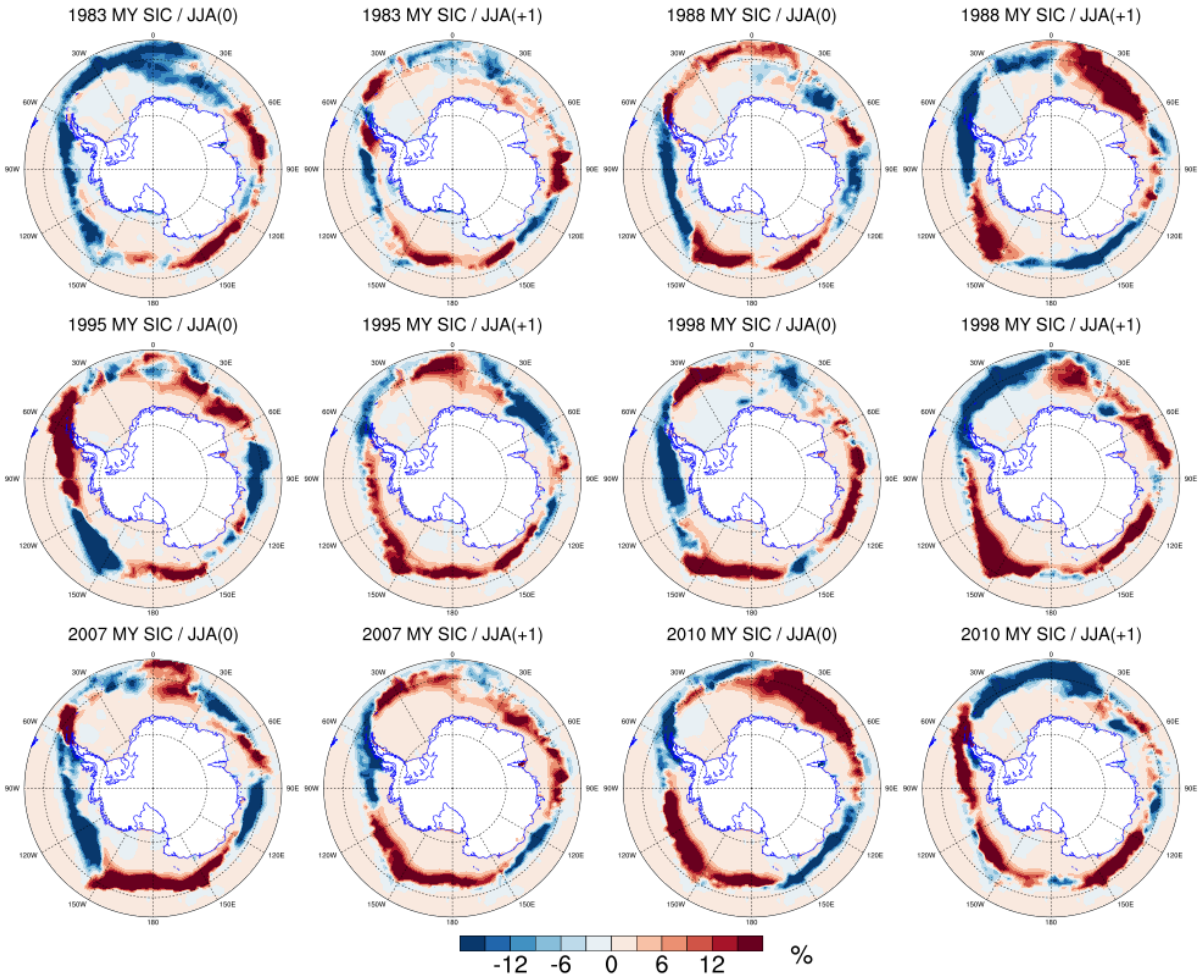

Reference

Kao, H. Y., & Yu, J. Y. (2009). Contrasting eastern-Pacific and central-Pacific types of ENSO. Journal of Climate, 22(3), 615-632.

Kim, J.-W. & Yu, J.-Y. (2022): Single- and multi-year ENSO events controlled by pantropical climate interactions, npj Climate and Atmospheric Science, DOI:10.1038/s41612-022-00305-y.

Saji, N. H., Goswami, B. N., Vinayachandran, P. N., & Yamagata, T. (1999). A dipole mode in the tropical Indian Ocean. Nature, 401(6751), 360.

Yu, J.-Y. & Kao, H.-Y. (2007). Decadal Changes of ENSO Persistence Barrier in SST and Ocean Heat Content Indices: 1958-2001. Journal of Geophysical Research, 112, D13106, doi: 10.1029/2006JD007654.